Characterization of the Interphase in PPO/PMMA Blends Compatibilized by P(S-*g*-EO)

H. Eklind, S. Schantz, and F. H. J. Maurer*

Department of Polymer Technology, Chalmers University of Technology, S-41296 Göteborg, Sweden

P. Jannasch and B. Wesslén

Department of Chemical Engineering II, Chemical Center, Lund Institute of Technology, P.O. Box 124, S-22100 Lund, Sweden

Received March 3, 1995; Revised Manuscript Received October 10, 1995[⊗]

ABSTRACT: The influence of a poly(styrene-*graft*-ethylene oxide) (P(S-*g*-EO)) copolymer on poly(2,6-dimethyl-*p*-phenylene oxide)/poly(methyl methacrylate) (PPO/PMMA) blends was studied by a number of different techniques in order to characterize the properties of the interphase. Scanning electron microscopy shows that the copolymer reduces the dispersed phase size, and dynamic mechanical spectroscopy (DMS) reveals a new micromechanical transition in the ternary blends. These effects are shown to be caused by a copolymer-rich interphase with a certain volume fraction and with its own characteristic properties. Solid-state nuclear magnetic resonance (NMR) relaxation times indicate that the poly(ethylene oxide) side chains of the copolymer are partially miscible with PMMA in the ternary blends, which suggests that the interphase does not only consist of pure copolymer.

1. Introduction

The blending of polymers is an attractive and practical technique to create materials with a wide variety of properties. As most polymer pairs are immiscible, they form multiphase systems with weak physical and chemical interactions across the phase boundaries. As a consequence, the rheology of the material will be strongly dependent on both the morphology and the interactions between the phases. Immiscible blends therefore often exhibit poor mechanical properties. In some cases, the addition of small amounts of "compatibilizers", e.g., block or graft copolymers which interact favorably with both major constituents, may alleviate this problem. The compatibilizer is considered to be located mainly at the interface between the two immiscible polymers, where in many cases it induces local miscibility. It may provide an increased adhesion and an enlarged volume of the interdiffusion layer, or "interphase", between the phases[1,2] and also reduce the interfacial energy between the phases and permit a more stable and finer dispersion.[3−5] These features of a compatibilizer result in a compatibilized blend morphology that is less sensitive to processing conditions and may also lead to improved mechanical properties.

The effect of compatibilizers on the phase structure of immiscible polymer blends has been investigated for many years. Early investigations focused mainly on immiscible binary blends of A and B homopolymers to which A−B block or graft copolymers were added, which is still of great interest today.[1,6−8] Later on, studies were made of blends with compatibilizers consisting of components where one was identical to one of the homopolymers and the other was chemically different but completely miscible with the other homopolymer (A−C copolymer).[2,9−10] More recently, investigations have studied blends of two immiscible homopolymers with C−D block copolymers, where A and B were miscible with the C and D block, respectively.[11−13]

The use of an A−B copolymer as a compatibilizer in an A/B blend involves a thermodynamically athermal process. The compatibilizing effect is then strongly dependent on the molecular masses of the individual blocks of the copolymers,[14] which should be equal to or higher than those of the corresponding homopolymers in order to obtain the most efficient compatibilization.[15,16] However, when one or two of the components in the copolymer are miscible with a homopolymer in an immiscible blend, an exothermic enthalpy of mixing between miscible pairs is likely to exist. This can be an important thermodynamic driving force in accomplishing the local miscibility in the interphase, and thus the compatibilizing effect, which means that a copolymer with components of low molecular masses in this case can function as an efficient compatibilizer.[16]

In this paper, the properties of the interphase in a ternary system are characterized by studying the influence of a graft copolymer on the viscoelasticity and the mobility in different blends. The studied system is based on poly(2,6-dimethyl-*p*-phenylene oxide) (PPO) and poly(methyl methacrylate) (PMMA) homopolymers, which form immiscible blends with weak interactions between the phases.[2] However, we expect that the properties of the PPO/PMMA blend change when a graft copolymer with polystyrene (PS) backbones and poly(ethylene oxide) (PEO) side chains is added, as previous reports have shown that binary PPO/PS[17] and PMMA/PEO[18−20] blends are miscible, at least in the melt, while the other combinations form immiscible blends.

We have utilized a number of different techniques to characterize the binary and ternary blends of PPO, PMMA and the poly(styrene-*graft*-ethylene oxide) copolymer on different length scales. The morphology and the macroscopic phase dimensions in the blends were studied by scanning electron microscopy (SEM). This method gives an indication of the interfacial activity of the copolymer but is difficult to use as a direct tool to study the extent and properties of the interphase. The dynamic mechanical properties of the individual components and the blends were examined in the solid and the melt state by dynamic mechanical spectroscopy (DMS), which is a useful tool to study both miscibility

* To whom correspondence should be addressed.
⊗ Abstract published in *Advance ACS Abstracts,* December 15, 1995.

0024-9297/96/2229-0984$12.00/0 © 1996 American Chemical Society

Table 1. Characteristics of the Graft Copolymer P(S-*g*-EO)

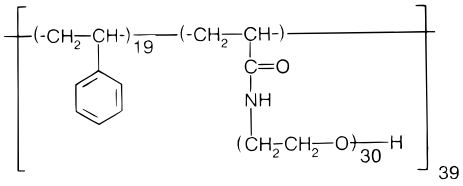

mole % acrylamide in the backbone	5
PEO content (wt %)	39
$\bar{M}_n$(backbone) (kg/mol)	80
$\bar{M}_n$(side chains) (kg/mol)	1.3
T_m of P(S-*g*-EO) (°C)	57
T_c of P(S-*g*-EO) (°C)	35

[a] The numbers 19, 30, and 39 given in the structure are average values.

on a microscopic length scale and the viscoelastic properties. Furthermore, solid-state nuclear magnetic resonance (NMR) techniques were employed to study the local structure and mobility in the blends.

This paper discusses the macroscopic and molecular structures of the blends, as well as the formation of an interphase with its own characteristic properties, together with the information gained from NMR and DMS measurements. A detailed comparison of the dynamic mechanical response of the studied blends with theoretical predictions using an interlayer model[21,22] is given elsewhere.[23,24]

2. Experimental Section

2.1. Materials. PPO and PMMA were both obtained from Scientific Polymer Products, Inc. PPO has a $\bar{M}_w$ of 50 kg/mol and a density of 1060 kg/m^3, while PMMA has a $\bar{M}_w$ of 75 kg/mol and a density of 1200 kg/m^3, according to the manufacturer. The PS−PEO graft copolymer, designated "P(S-*g*-EO)" (also used elsewhere[23,24]), was prepared by ethoxylation of an amide-containing styrene copolymer. The styrene backbone copolymer was synthesized by free-radical polymerization of styrene and acrylamide. Grafting was achieved by first ionizing the amide groups with potassium *tert*-butoxide and then using them as initiating sites for anionic polymerization of ethylene oxide. The grafting polymerization was performed in 2-ethoxyethyl ether at 80 °C and at an EO pressure of 5 bars. P(S-*g*-EO) was purified by precipitation from the reaction mixture in cold diethyl ether. After drying, the precipitate was washed repeatedly with distilled water to remove homo-PEO and potassium salts. The purity was checked by size exclusion chromatography (SEC). Structural and thermal characteristics of P(S-*g*-EO) are listed in Table 1. The content of grafting sites, i.e., acrylamide units, in the backbone copolymer was determined by comparing the IR absorption bands at 1680 cm^{-1} (carbonyl groups in acrylamide units) and at 1610 cm^{-1} (phenyl groups in acrylamide units) of the backbone copolymer. The molecular mass of the backbone copolymer was determined by SEC, using tetrahydrofuran (THF) as eluent and polystyrene standards for calibration. To eliminate the anomalous elution behavior of the backbone copolymer, the primary amide groups were alkylated with isopropyl bromide prior to SEC analysis. The EO content of P(S-*g*-EO) was determined from ^{1}H NMR. The molecular mass of the PEO side chains was calculated by means of knowledge of the content of grafting sites in the backbone copolymer and of the EO content in P(S-*g*-EO). The melting and crystallization of the PEO part of P(S-*g*-EO) were studied by DSC. The sample was first heated from room temperature to 100 °C, then cooled to −100 °C, and finally reheated to 100 °C. The scanning rate was 5 °C in all experiments. The crystallization temperature given in Table 1 corresponds to the temperature at the onset of crystallization during cooling, while the melting temperature corresponds to the peak temperature in the second heating scan. More details of the preparation, purification, and characterization of P(S-*g*-EO) have been described previously.[25]

2.2. Blending Procedure. Before blending, both PPO and PMMA were dried overnight at 60 °C, while P(S-*g*-EO) was dried in a vacuum oven at 40 °C for 20 h. The blends were prepared in a Brabender AEV 330 with a chamber volume of 50 cm^3. Blending was performed with a set temperature of 260 °C and a mixing time of 10 min, after which the blends were cooled at room temperature. One disadvantage is that the blending temperature is above the reported decomposition temperature of PMMA[26] at approximately 200 °C, but these conditions were necessary in order to obtain a proper mixing. Blends of PPO and PMMA, with the common composition of 30 volume parts of PPO and 70 volume parts of PMMA, were prepared with an additional amount of 0, 1, 2, 5, or 10 volume parts of P(S-*g*-EO). Two binary PPO/P(S-*g*-EO) and PMMA/P(S-*g*-EO) blends, both with a volume composition of 100/10, were also prepared in order to study the interactions between the copolymer and each of the two homopolymers. Experimental samples were prepared by compression molding the Brabender blends. The volume compositions referred to in the text are based on the densities at room temperature. The density of the copolymer was estimated to be 1110 kg/m^3 by taking the weight-average values at room temperature of PS (1060 kg/m^3) and PEO (1210 kg/m^3), respectively.

2.3. Instrumentation. SEC. The effect of the blending procedure on the molecular mass distribution was examined by size exclusion chromatography (SEC). The equipment consisted of a Waters 510 pump, a column oven, a Waters 712 wisp autoinjector, and a Waters 410 refractive index detector. The experiments were performed in chloroform at 30 °C with the use of two commercial Styragel columns from Polymer Laboratories, and narrow PS standards were used for calibration. The sample concentration was 1 g/L, and the samples were filtered through 0.45 filters before injection. The experiments indicated that processed PPO differed slightly from unprocessed PPO; i.e., the amount of the low molecular mass part decreased while the amount of the high molecular mass part increased with processing. At the same time, the $\bar{M}_w/\bar{M}_n$ quotient decreased from 4.4 to 4.0. The SEC chromatograms of pure PMMA showed no significant change in average molecular mass or molecular mass distribution after processing as compared with the unprocessed samples. Both unprocessed and processed PMMA had a $\bar{M}_w/\bar{M}_n$ of 2.3. It was not possible to make a similar comparison between unprocessed and processed P(S-*g*-EO) due to the limited amount of compatibilizer available.

SEM. A Zeiss DSM 940A scanning electron microscope (SEM) was used to analyze the phase structure of the blends. The blends were first fractured in liquid nitrogen. The samples were then fixed to the substrate, sputter-coated with a thin gold layer, and finally analyzed under an electron microscope. Both compression-molded samples and original Brabender blends were analyzed.

DSC. Differential scanning calorimetry (DSC) measurements of the pure constituents as well as the binary and ternary blends were performed with a Perkin-Elmer System 7. The procedure of the analysis of P(S-*g*-EO) is described above, while all other experiments were performed as follows. The samples were first heated from room temperature to 130 °C, after which they were cooled with a scanning rate of 5 °C/min to −80 °C, and finally heated again with a scanning rate of 5 °C/min to a temperature above the T_g's of the constituents of each sample. The DSC data given in the text below correspond to the second heating scan.

DMS. The dynamic mechanical spectroscopy (DMS) experiments were performed with a Rheometrics RDA II dynamic analyzer in the oscillatory mode. Samples were prepared by compression molding. The solid-state samples with the shape of a rectangular parallelepiped had the common approximate dimensions of 30 × 12 × 2 mm, while the melt-state cylindrical samples had a diameter of 25 mm and an approximate thickness of 2 mm. After preparation, the samples were kept dry in a desiccator. Strain sweeps were first performed in order to ensure that the measurements were obtained in the viscoelastic region. The strain was 0.1% for the rectangular

samples, except for the PMMA/P(S-*g*-EO) 100/10 blend, which was subjected to a strain of 0.2%. The circular disks were subjected to a maximum strain of 10%. Angular frequency (ω) sweeps were then performed from 500 to 0.02 rad/s (0.001 rad/s for certain samples and temperatures) with a step size of up to 10 points per decade. For the sake of simplicity, only the values at the angular frequency of 0.02321 rad/s are given in the text and figures when nothing else is indicated. The samples were scanned at temperatures (T) ranging from −80 to +250 °C. The measurements were performed with different temperature steps in different temperature regions, but only the data at every 5 °C are given in the figures. The measurements in the temperature range from 25 to 150 °C were performed by starting at 150 °C and then decreasing the temperature, while all other measurements were performed by starting at a lower temperature and then increasing the temperature. This was done because the effect of any crystalline part of PEO, above the onset of crystallization at approximately 35 °C in pure P(S-*g*-EO) (as measured by DSC), should be eliminated.

Solid-State NMR. CPMAS (cross polarization magic angle spinning) experiments were performed on a Varian VXR300 spectrometer, operating at 75.4 and 299.9 MHz for ^{13}C and ^{1}H, respectively. The samples were packed in silicon nitride rotors with Torlon end caps and spun at 5.1 kHz in a Varian probe of Jacobsen design. The sample temperature was maintained at ~28 °C in most of the experiments. Chemical shifts were calibrated via external reference to the aromatic carbon of hexamethylbenzene (132.2 ppm relative to TMS).

Cross polarization was performed at 36 kHz (7 μs $\pi/2$ pulses for ^{13}C and ^{1}H), the proton decoupling strength was approximately 70 kHz, and the delay between successive acquisitions was 3 s. Some direct polarization MAS spectra (with high-power proton decoupling) were also obtained following a single ^{13}C $\pi/2$ pulse and with a recycle delay varied between 0.5 and 20 s.

Proton rotating frame relaxation times, $T_{1\rho}$(H), were obtained by spin-locking the protons for a variable time before cross polarization and detection through the carbons.[27] Carbon $T_{1\rho}$(C)'s were determined by varying the carbon spin-lock time after cross polarization.[28] A cross polarization contact time between 0.1 and 1 ms was used in most of the relaxation time experiments. For each spectrum in the arrayed experiments, 1000−8000 FID's were accumulated, repeatedly cycling through the different time values. This corresponds to measurement times up to 96 h for the determination of one relaxation decay.

3. Results and Discussion

3.1. Viscoelasticity and Morphology. Viscoelastic Characteristics of the Pure Blend Constituents. The experimental dynamic mechanical values of the dynamic shear modulus, $G_d(\omega,T)$, and the loss factor, tan $\delta(\omega,T)$, for PPO, PMMA, and P(S-*g*-EO) are shown (for ω = 0.02321 rad/s) in Figure 1a,b. It can be observed that PPO homopolymer has an approximately constant G_d level up to its glass transition, where it has a maximum in tan δ at 214 °C (G'' maximum at 207 °C). The G_d for PMMA is higher than for PPO at lower temperatures and is also approximately constant up to its α-transition. The maximum in tan δ of PMMA occurs at 108 °C (G'' maximum at 100 °C), and the upper part of the β-transition can be observed on the low-temperature side of Figure 1b.

The copolymer behaves quite differently than the homopolymers, as can be observed in Figure 1a,b. When measurements were performed on P(S-*g*-EO) (from lower to higher temperatures) below room temperature, where it is partially crystalline, it was possible to detect a maximum in G'' at −56 °C (ω = 1 rad/s). The position of this loss maximum is in agreement with data in the literature[29] and corresponds to the glass transition of the amorphous PEO chains. A weak and broad peak in G'' was also observed between −20 and +30 °C. The position of this peak could not be accurately determined in a tan δ vs temperature plot, as it was overlapped by the losses corresponding to the melting. To eliminate the influence of melting of P(S-*g*-EO), measurements were also performed from higher to lower temperatures at temperatures at which it was completely amorphous. In this experiment, P(S-*g*-EO) has a modulus that is much lower than both the moduli of the homopolymers. A maximum in G'' could not be detected for P(S-*g*-EO) in the temperature range from 25 to 230 °C, but it showed a small peak in tan δ with a maximum at approximately 35 °C (determined by measuring at higher temperatures and lower frequencies with the use of frequency−temperature superposition) after which tan δ rose sharply, as can be observed in Figure 1b. This loss maximum might correspond to a relaxation mechanism of the PS backbones.

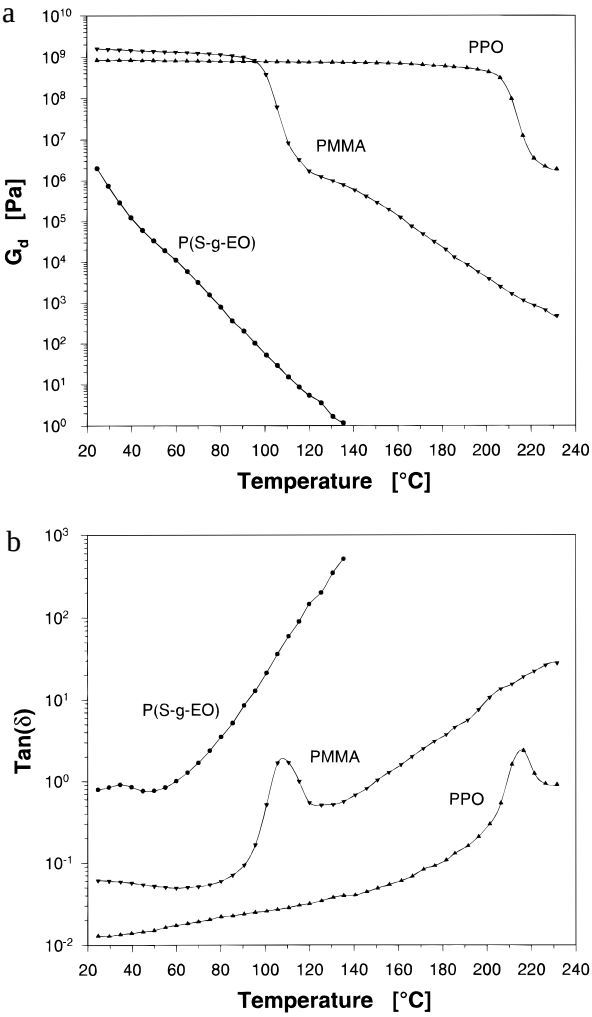

Figure 1. (a) Dynamic shear modulus, $G_d(\omega,T)$, and (b) loss factor, tan $\delta(\omega,T)$, of PPO (▲), PMMA (▼), and P(S-*g*-EO) (●) at different temperatures.

Binary PPO/P(S-*g*-EO) and PMMA/P(S-*g*-EO) Blends. Binary PPO/P(S-*g*-EO) and PMMA/P(S-*g*-EO) blends were also studied by DMS, and the results are shown in Figure 2. The PMMA/P(S-*g*-EO) 100/10 blend shows a single T_g in the temperature range from −80 to +250 °C, with a maximum in G'' at 93 °C (tan δ maximum at 105 °C), which is lower than for PMMA. The PPO/P(S-*g*-EO) 100/10 blend also shows a single maximum in G'' in this temperature range at a temperature of 187 °C (maximum in tan δ at 203 °C). It can observed that the T_g's of the two binary blends are both lower, and the tan δ curves of the binary blends

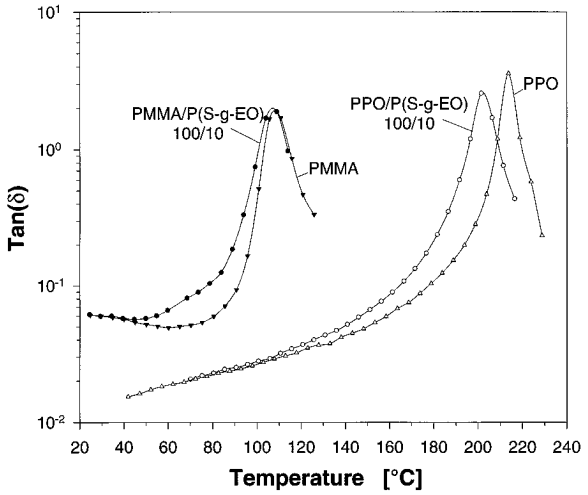

Figure 2. Experimental values of tan δ for PMMA (▼), PMMA/P(S-*g*-EO) 100/10 (●), PPO (△), and PPO/P(S-*g*-EO) 100/10 (○) at different temperatures.

are distinctly broader on the low-temperature side of the maxima, as compared with pure PMMA and PPO homopolymers. This can be explained by the fact that the PS and the PEO parts of P(S-*g*-EO) interact with PPO and PMMA, respectively (PS and PEO have T_g's lower than PPO and PMMA, respectively), which causes the copolymer to be at least partially miscible with both PPO and PMMA. Consequently, these experiments imply that P(S-*g*-EO) may function as a suitable compatibilizer in the PPO/PMMA system. This is also supported by the fact that no melting or crystallization was detected for PEO in the binary blends by DSC or DMS measurements.

Ternary PPO/PMMA/P(S-*g*-EO) Blends. SEM micrographs of the binary PPO/PMMA 30/70 blend and the ternary PPO/PMMA/P(S-*g*-EO) 30/70/10 blend are shown in parts a and b of Figure 3, respectively. In the PPO/PMMA 30/70 blend, the PPO phase is observed to form approximately spherical inclusions in a matrix of PMMA. This structure is also preserved when P(S-*g*-EO) is added, but the PPO phase dimension is then clearly decreased. The average dimensions of the inclusions and holes (approximately 30 particles measured for each sample, the error bars representing the standard deviation), as determined from SEM micrographs of fracture surfaces of the PPO/PMMA/P(S-*g*-EO) 30/70/Φ blends, are given in Figure 4 as a function of volume parts of P(S-*g*-EO) (Φ). The results show that the average particle diameter decreases continuously with an increasing amount of added compatibilizer. These results suggest that at least a major part of the copolymer is concentrated at the interphase between PPO and PMMA.

To get an indication of the thickness of the interphases in the PPO/PMMA/P(S-*g*-EO) 30/70/Φ blends, we used the average particle diameters of the inclusions and holes given in Figure 4 and assumed that all the added copolymer formed a uniform interphase between the PMMA matrix and the PPO particles. The estimated interphase thickness is then approximately 47 ± 10 nm for all copolymer compositions. The variation of the thickness with the amount of copolymer is small considering the large variation in the ratio between the particle diameters and the estimated interphase thickness (20−200).

tan δ values are shown in Figure 5 as a function of temperature for the PPO/PMMA/P(S-*g*-EO) 30/70/0, 30/70/1, 30/70/2, 30/70/5, and 30/70/10 blends, together with a theoretical prediction of a 30/70/2 blend (dotted line). It can be observed that PPO/PMMA/P(S-*g*-EO) 30/70/0 has a maximum in tan δ at approximately 111 °C, which is slightly above the maximum at 108 °C of pure processed PMMA. The blend also has a maximum in tan δ at 212 °C (not shown in the figure), which corresponds to the glass transition of PPO. The blends with the added graft copolymer display an, at first, unexpected behavior. In addition to the two α-transitions of the two main constituents, i.e., PPO and PMMA, an additional relaxation mechanism below the glass transition temperature of PMMA can be observed in the

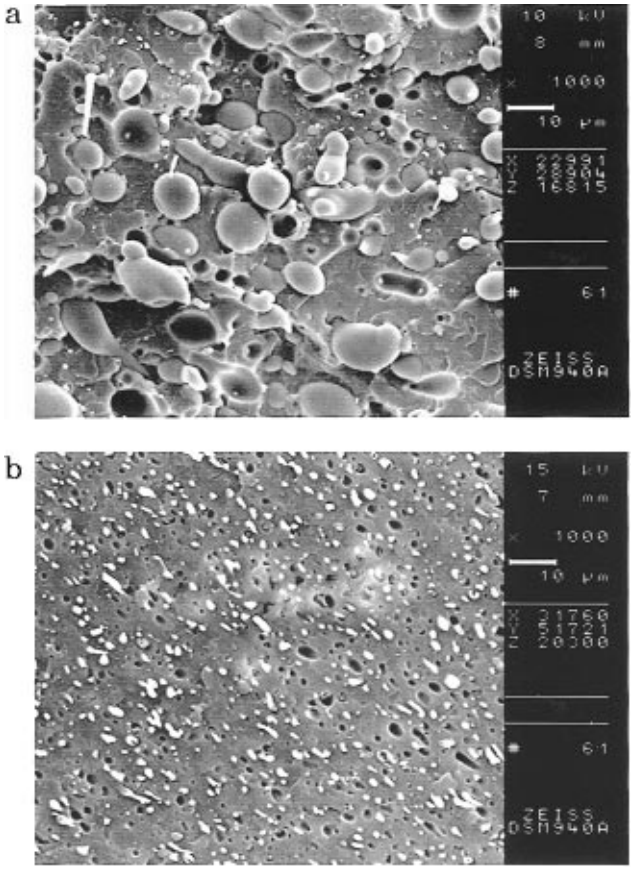

Figure 3. SEM micrographs of fracture surfaces of (a) PPO/PMMA 30/70 and (b) PPO/PMMA/P(S-*g*-EO) 30/70/5.

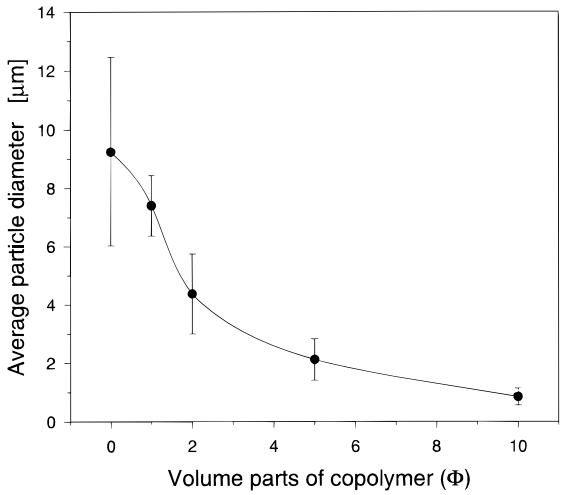

Figure 4. Average diameters of the inclusion and holes in the PPO/PMMA/P(S-*g*-EO) 30/70/Φ blends (Φ = 0, 1, 2, 5, and 10), as determined from SEM micrographs of fracture surfaces. The error bars represent the standard deviations.

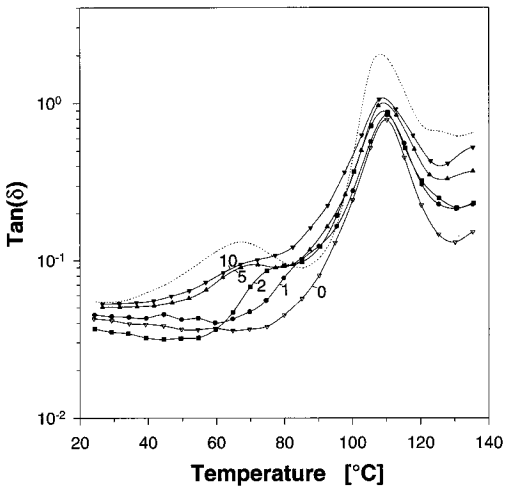

Figure 5. Experimental data of tan δ vs temperature for the PPO/PMMA/P(S-*g*-EO) 30/70/Φ system, where Φ is 0 (▽), 1 (●), 2 (■), 5 (▲), and 10 (▼). The dotted line represents the calculated values for the theoretical PPO/PMMA/P(S-*g*-EO) 30/70/2 blend, assuming that PPO forms spherical particles in a matrix of PMMA, with P(S-*g*-EO) as an interphase between PPO and PMMA.

ternary system. The temperature position of the additional transition, as well as its shape and size, depends on the amount of P(S-*g*-EO) added. With increasing amounts of copolymer, the transition clearly shifts to lower temperatures. The ternary blend with 1 volume part of P(S-*g*-EO) added shows an additional relaxation between 90 and 100 °C, which partially overlaps the PMMA glass transition. If the P(S-*g*-EO) content is increased to 2 or 5 volume parts, the transition is further separated from the PMMA peak, i.e., the additional peak is shifted to lower temperatures, while the position of the PMMA peak does not shift. In the PPO/PMMA/P(S-*g*-EO) 30/70/10 blend, the position of the additional peak is the same as the position in the 30/70/5 blend (observed more clearly in a G'' vs temperature plot). The only difference between these two blends is a broadening of the PMMA transition toward lower temperatures for the 30/70/10 blend.

The existence of an additional transition for the PPO/PMMA/P(S-*g*-EO) system is an interesting phenomenon. From the viscoelastic data of the constituents of the blends, it can be observed that only the pure homopolymers show distinct transitions above room temperature. P(S-*g*-EO), on the other hand, has a maximum in G'' only at −56 °C (ω = 1 rad/s), but also a very small maximum in tan δ at 35 °C (ω = 0.02321 rad/s). The additional peak in tan δ has seemingly no direct relation with any relaxation mechanism in the constituents present in the PPO/PMMA/P(S-*g*-EO) system.

In Figure 5, the experimental viscoelastic observations of the PPO/PMMA/P(S-*g*-EO) blends are compared with a theoretical simulation (dotted line), which is a calculation of the temperature-dependent dynamic mechanical properties of a 30/70/2 blend by the use of an interlayer model.[21−23] The model contains a spherical particle (PPO) surrounded by a shell of interphase (P(S-*g*-EO)), which in turn is covered by a shell of matrix material (PMMA), which finally is surrounded by blend material. In the calculations, we use the dynamic shear complex modulus of PPO and PMMA as input data for the particles and matrix, respectively. By using the dynamic shear complex modulus of P(S-*g*-EO) as input data for the interphase, an additional mechanical relaxation is predicted in accordance with experiments, as is shown in Figure 5. The observed additional transition does not represent a transition corresponding to any of the pure constituents. Instead it should be considered as a "micromechanical transition", i.e., a transition which results from the combined influence of the microstructure of the blend including an interphase and the relative temperature-dependent moduli of the blend constituents. The position of the micromechanical transition is predicted at temperatures below the glass transition temperature of PMMA. The position depends on the volume fraction of the interphase, with a shift to lower temperatures when the volume fraction of interphase material is larger,[23] in qualitative accordance with experiments shown in this paper. A discrepancy between theory and experiments is the predicted position of the micromechanical transition at lower temperatures than what is experimentally observed. A quantitative agreement between theory and experiment can only be achieved by assuming that the interphase has properties which are shifted approximately 10 °C to higher temperatures. The difference between experiments and theory, using the original P(S-*g*-EO) data for the interphase, could thus be qualitatively explained by a shift of the T_g of P(S-*g*-EO) to higher temperatures due to miscibility in the interphase between the PS and/or PEO segments and the PPO and PMMA homopolymers, respectively. This assumption is strengthened by the observation of partial miscibility in the two binary PPO/P(S-*g*-EO) 100/10 and PMMA/P(S-*g*-EO) 100/10 blends.

The ability to use the interlayer model, with an interphase between the particles and the matrix, using only the original experimental complex shear moduli of the pure constituents and the volume fractions, to simulate the dynamic mechanical response of the ternary blends in good agreement with experiments, is a strong indication that an interphase with a certain volume and specific properties actually exists. It should be noted that the existence of the micromechanical transition is predicted by the introduction of P(S-*g*-EO) as interphase material, even though the copolymer itself does not show a transition in that temperature region. The assumption of an interphase between PPO and PMMA, created by the P(S-*g*-EO) copolymer, is also in accordance with other observations. The position of the tan δ maximum of PMMA and PPO is affected only negligibly by the addition of 1 or 2 volume parts of P(S-*g*-EO). However, when more than 5 volume parts of copolymer are added to the PPO/PMMA 30/70 blend, the PMMA peak becomes broader on the low-temperature side, while the position of the additional maximum is less affected, which can be observed in Figure 5. A reduction of the peak temperature of tan δ for PPO in the ternary blends could also be detected, from 212 °C without P(S-*g*-EO) to 200 °C with an added 5 volume parts of P(S-*g*-EO). A similar reduction of T_g for both PPO and PMMA was also indicated by DSC, especially for the blends with the high copolymer contents. This could also be an indication of a concentration of the copolymer at the interphase when small amounts of copolymer are added (1 or 2 volume parts), but that an extra addition of copolymer results in the dissolution of more copolymer in the PPO and PMMA phases.

3.2. Molecular Structure and Mobility. Solid-state NMR was employed to characterize the structure on a molecular level and the local mobility of the blends, using the CPMAS technique to obtain ^{13}C spectra and various relaxation times. In the case of blend constitu-

Table 2. Proton $T_{1\rho}$(H)[a] Values (ms) for P(S-*g*-EO), PPO, PMMA, and Their Blends at 28 °C

PPO/PMMA/P(S-*g*-EO)	PPO[b]	PMMA[b]	P(S-*g*-EO)[c]
0/0/100			0.2, 1.3
0/100/10		6	0.5, 5
100/0/10	14		0.5, 9
30/70/0	14	6	
30/70/1	13	5	
30/70/2	14	6	
30/70/5	13	6	0.3 ± 0.1, 4 ± 2
30/70/10	12	6	0.5, 5

[a] Estimated accuracy: for decays fitted to single exponentials ±10%; for decays fitted to biexponentials ±20% or otherwise explicitly given. [b] Average for all resolved signals. [c] PEO resonance of P(S-*g*-EO) only.

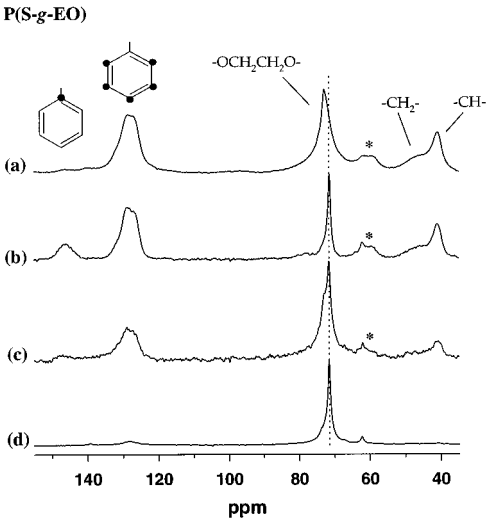

Figure 6. Room-temperature ^{13}C NMR spectra of P(S-*g*-EO): CPMAS spectra with CP time 50 μs (a) and 4 ms (b); MAS spectra with recycle delay 20 s (c) and 0.5 s (d). Spinning sidebands are marked with an asterisk (5.1 kHz MAS frequency). The dashed line indicates the peak position of the amorphous PEO component.

ents of high concentrations, PPO and PMMA, we found in these measurements very weak sensitivity to the addition of P(S-*g*-EO) with changes close to the experimental accuracy (see, for example, Table 2). This is in agreement with the previously discussed results, which indicate that the addition of copolymer does not change the level of miscibility between PPO and PMMA. The following section is therefore focused on the behavior of the PEO side chains of P(S-*g*-EO), for which we observed significant effects in the binary and ternary blends (the signals from the PS backbone of the copolymer are not completely resolved in the blends). A sensitivity problem however arises for blends with copolymer contents below ~5−10%, due to the low natural abundance of carbon-13. For these blends, isotope enrichment would be necessary for reliable measurements of intensities.

3.2.1. ^{13}C NMR Spectra. Figure 6 shows ^{13}C spectra of pure P(S-*g*-EO) obtained under various experimental conditions. The CPMAS spectra reveal that the PEO resonance is composed of more than one component. At short cross polarization (CP) contact times, a broader component at ~73 ppm is the more intense (Figure 6a), whereas at longer contact times a narrower component at ~71 ppm dominates (Figure 6b). This is because the relative area of two components changes as the CP time is varied due to the difference in both CP rate and $T_{1\rho}$(H) relaxation time; the low-field component has the higher CP rate (maximum intensity

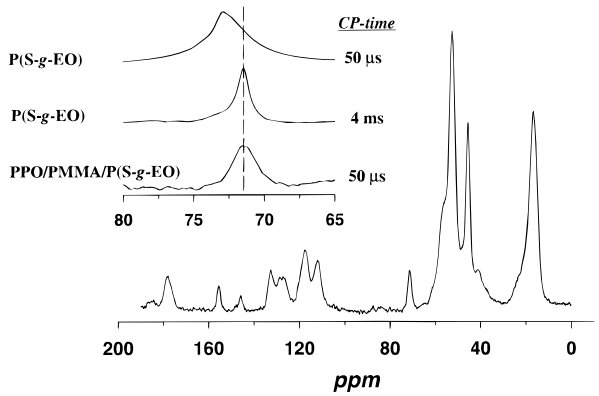

Figure 7. Room-temperature ^{13}C CPMAS NMR spectrum of a PPO/PMMA/P(S-*g*-EO) (30/70/10) blend (CP time = 50 μs). The inset shows expansions of the PEO region for the blend (bottom) and for pure P(S-*g*-EO) (top and middle spectra taken from Figure 6a,b, respectively).

at ~100 μs as compared with ~800 μs for the component at higher fields) and the shorter $T_{1\rho}$(H) (see next paragraph).

An alternative approach for identifying the two spectral components of the PEO side chains is based on their different carbon T_1(C) relaxation times. Spectra c and d in Figure 6 were obtained using direct carbon polarization (no CP) with recycle delays of 20 and 0.5 s, respectively. Major contributions to the intensity of spectrum d in Figure 6 are from those carbons with short T_1's. Because of the long T_1(C) of the low-field component (several seconds) of PEO, it is dramatically suppressed; see spectrum d in Figure 6. The resonances of the styrene backbone also show significantly reduced intensities with a short delay time. The weak signal at ~61 ppm in spectrum d (less pronounced in spectra b and c) is attributed to the ~CH_2OH end group of the side chains.[30]

We assign the two dominant copolymer peaks at ~73 and ~71 ppm to crystalline and amorphous side chains, respectively, similar to reports on pure PEO.[31−33] The large difference in mobility between crystalline and amorphous regions above the glass transition temperature is demonstrated in the spectra in Figure 6. The crystalline PEO segments show a higher CP rate than the amorphous segments, as the proton to carbon CP transfer is enhanced by static ^{1}H−^{13}C dipolar interactions (Figure 6a,b). Molecular motions in the amorphous domains result in reasonably short carbon T_1 values, while the low mobility in the crystalline regions leads to much longer T_1's. The crystalline component is therefore suppressed in the spectrum obtained with a short recycle delay (Figure 6d). Note that the main chain styrene carbons also have greatly reduced intensities in Figure 6d, which indicates a lower mobility as compared with the amorphous side chains. Finally, MAS spectra of the PEO region obtained above the melting temperature show a motionally narrowed resonance at 71.5 ppm, in agreement with our assignment.

Next we turn to the spectra of the blends. A carbon-13 CPMAS spectrum of the PPO/PMMA/P(S-*g*-EO) 30/70/10 blend is given in Figure 7. Unfortunately, most of the copolymer resonances in the blends are overlapped by the more intense peaks of PPO (quaternary carbons at 155, 146, and 133 ppm; protonated aromatic at 117 and 112 ppm; methyl at 16 ppm) and PMMA (carbonyl carbons at 178 ppm; methoxy at 52 ppm; quaternary at 45 ppm; α-methyl at 17 ppm). Only the PEO peak at ~71 ppm is completely resolved. This

resonance changes significantly upon blending; in spectra taken with the same CP time of 50 μs, the peak shifts ~2 ppm to higher fields in the blends (see inset in Figure 7). Clearly, the chemical shift of the PEO peak in the blend corresponds to the amorphous side chain component in the spectra of pure P(S-*g*-EO). The same chemical shift (within the experimental accuracy) was found for the PEO resonance in all binary and ternary blends investigated in the present study, which indicates the absence of crystalline ordering, in agreement with the results from DSC and DMS experiments. A broadening however occurs in the NMR spectra upon blending; e.g., the full width at half-height was found to be ~120 Hz for the PEO resonance in the PPO/PMMA/P(S-*g*-EO) 30/70/10 blend (independent of CP time) as compared with approximately 50 Hz for the amorphous component in pure P(S-*g*-EO) (see Figure 7). The origin of the spectral broadening could be a wider distribution of local environments for the copolymer side chains in the blends, which is either narrower or averaged by molecular motion in the amorphous regions of pure P(S-*g*-EO).

3.2.2. NMR Relaxation Times. Relaxation times were measured to further characterize the side chains of P(S-*g*-EO) in the blends: namely, proton ($T_{1\rho}$(H)) and carbon ($T_{1\rho}$(C)) rotating frame spin−lattice relaxation times. In the case of protons, their relaxations are sensitive to domain sizes or level of mixing, as spatial transport of magnetization, spin diffusion, between neighboring protons acts as an efficient averaging mechanism.[34] Because of the $1/r^6$ internuclear distance dependence of the spin diffusion rate, magnetization transfer is limited to molecular distances. For example, in a binary polymer blend, the observation of a single averaged $T_{1\rho}$(H) indicates phase dimensions smaller than the order of ~1 nm, i.e., molecular miscibility.[27,35]

Carbon $T_{1\rho}$'s, on the other hand, are not influenced by spin diffusion as the average distance between carbon-13 spins is relatively large.[28] $T_{1\rho}$(C) relaxation times can therefore be used to extract information about molecular mobility in the midkilohertz region of specific sites within a molecule. A complication may arise for some systems because of nonmotional (spin−spin) contributions to the relaxation. The carbon spins are relaxed by proton spin fluctuations; for spin−spin contributions, the proton fluctuations are caused by changes in spin state rather than by molecular motion. Spin−spin processes are especially important for rigid systems, such as crystalline regions of polymers.[28] However, $T_{1\rho}$(C) for salt-complexed amorphous PEO, of interest in the present study, has been shown to be dominated by motional (spin−lattice) relaxation above the glass transition temperature.[36] Therefore, we interpret $T_{1\rho}$(C) for the amorphous PEO groups of P(S-*g*-EO) as a motional parameter (using a spin-lock field $\omega_{1C}/2\pi = 36$ kHz, which is close to that used in ref 36).

Pure P(S-*g*-EO). Figure 8 and Table 2 show results from the proton $T_{1\rho}$(H) measurements of P(S-*g*-EO) (together with results from the blends, to be discussed later). The relaxation time is given by the inverse slope of the logarithmic carbon intensity decay. Clearly, the PEO relaxation cannot be described by a single-exponential process (see Figure 8). The short and long time decays can be identified with crystalline and amorphous domains, respectively, based on the continuous change in line shape as the proton spin-lock time increases. For example, after a spin-lock time of 6 ms, the band envelope is dominated by the amorphous component,

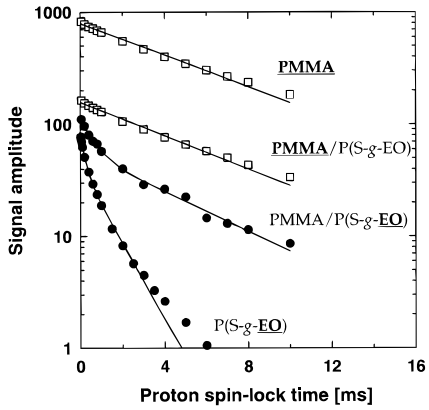

Figure 8. Proton $T_{1\rho}$(H) relaxation behavior at ~28 °C for PMMA, P(S-*g*-EO) (PEO resonance), and a PMMA/P(S-*g*-EO) (100/10) blend. The solid lines are single or biexponential fits to the data. For clarity, each decay is begun at a separate origin on the *y*-axis.

Table 3. Carbon $T_{1\rho}$(C) Values (ms) for P(S-*g*-EO) in Blends with PPO and PMMA at 28 °C

PPO/PMMA/P(S-*g*-EO)	P(S-*g*-EO)[a]
0/0/100	0.4, 2.1
0/100/10	3
100/0/10	5
30/70/5	3 ± 1
30/70/10	3

[a] PEO resonance of P(S-*g*-EO) only. Estimated accuracy ±20% or otherwise explicitly given.

due to the loss of the faster relaxing crystalline component. For the present discussion, we use as a first approximation a sum of two exponentials (time constants 0.2 and 1.3 ms) to fit the data, although the discrepancy at the long time end in Figure 8 indicates that at least three exponential terms are needed to describe the PEO magnetization decay (a three-exponential fit gives time constants 0.1, 0.7, and 2.4 ms). The main chain styrene protons of the copolymer relaxes more slowly than the side chains at room temperature, and with a less pronounced nonexponentiality.

The $T_{1\rho}$(C) relaxation for PEO is similar to the proton relaxation (see Table 3). Again we find a decaying ^{13}C magnetization, which is the sum of at least two exponentially decreasing components. From decomposition into two exponentials, the faster relaxation (0.4 ms) is attributed to crystalline and the slower (2.1 ms) to amorphous side chains. As for $T_{1\rho}$(H), the assignment is based on the change in line shape as the carbon spin-lock time varies.

Binary PPO/P(S-*g*-EO) and PMMA/P(S-*g*-EO) Blends. The proton $T_{1\rho}$(H) relaxation for the copolymer side chains changes dramatically in blends with PMMA and PPO (see Table 2 and Figure 8). The magnetization decay for PEO is well fitted to a biexponential function, however with a lower overall rate than for pure P(S-*g*-EO). Note that the whole PEO decay curve for the blends corresponds to amorphous side chains. This can be recognized both from the spectral line shape (see above) and from the absence of the very fast crystalline decay (see Figure 8). In none of the binary blends are the relaxation of PEO and the majority component equal, which implies that the domain sizes are too large for spin diffusion to completely average the relaxations. This is not surprising, as we expect that heterogeneities are present in the blends, at least on the nanometer length scale probed in the $T_{1\rho}$(H) experiment. However, in the case of PMMA/P(S-*g*-EO), the longer $T_{1\rho}$(H)

component for PEO is close to the PMMA relaxation time (see Table 2). The relaxations are, in fact, similar to results recently reported[37] for melt-mixed PMMA/PEO blends of comparable compositions (amorphous blends with low amounts of PEO). In the latter system, the $T_{1\rho}$(H) decay for PEO was found to be nonexponential over a large range of compositions. An explanation for the relaxation behavior in both PMMA/PEO and PMMA/P(S-*g*-EO) blends may be that the blends contain microscopic regions of PEO segments mixed with PMMA (long $T_{1\rho}$(H) decay) as well as separated domains (short $T_{1\rho}$(H) component). It is also possible however that the PEO proton decay does not reflect physically distinct regions; i.e., there is not necessarily a 1:1 correlation between the number/amplitude of observed relaxation components and the number/fraction of regions present in the material. Complex nonexponential relaxation may arise if the rate of spin diffusion is comparable to the difference in relaxation rates of the components.[38] A further complication for the PMMA/P(S-*g*-EO) blend is that spin diffusion in/out of styrene-rich regions may contribute to the observed relaxation. Nevertheless, even though the exact origin of the PEO $T_{1\rho}$(H) decay is uncertain, it appears that the relaxation is affected by spin diffusion to PMMA and hence it reflects at least some molecular contact between PEO and PMMA segments. If the P(S-*g*-EO) was completely phase-separated in the PMMA matrix, we would expect the PEO relaxation in the blend to resemble that of pure P(S-*g*-EO). The unchanged PMMA relaxation upon blending (Figure 8 and Table 2) does not contradict the scenario of some mixing, as the PEO concentration is too low to significantly speed up the PMMA relaxation through spin diffusion, assuming simple averaging of relaxation rates. The PEO relaxation is different in the PPO/P(S-*g*-EO) 100/10 blend (see Table 2), which also gives some support for the idea of partial mixing, inasmuch as we do not expect PPO and PEO to be miscible.

The carbon $T_{1\rho}$(C) relaxation for the copolymer side chains also changes in the blends with PMMA and PPO (see Table 3). Interestingly, the nonexponential $T_{1\rho}$(C) character is lost upon blending, and the PEO magnetization decays are single exponential within the experimental accuracy. The observation is in agreement with the absence of side chain crystallinity, as previously discussed, and it indicates that the biexponential *proton* $T_{1\rho}$(H)'s are indeed affected by spin diffusion and are not the result of two amorphous side chain populations which differ in mobility ($T_{1\rho}$(C) and $T_{1\rho}$(H) are sensitive to molecular motions with correlation times in about the same time window). $T_{1\rho}$(C) values for PEO in the blends are longer than the amorphous component for pure P(S-*g*-EO), which implies a changed mobility for the side chains (Table 3). When further comparing the carbon relaxation times for PEO in the PPO/P(S-*g*-EO) 100/10 and PMMA/P(S-*g*-EO) 100/10 blends, we find a difference of almost a factor of 2; $T_{1\rho}$(C) for the former system (5 ms) is close to that for pure PEO (amorphous component of a high molecular weight sample) and $T_{1\rho}$(C) for the latter blend (3 ms) is close to that for amorphous PMMA/PEO blends of comparable composition.[39] The observed difference in mobility may thus be a result of mixing between PEO side chains and PMMA, in agreement with the proton $T_{1\rho}$(H) results (Figure 8) and with the dynamic mechanical data (Figure 2). For a more extensive comparison of midkilohertz mobilities in the blends, relaxation time measurements at several temperatures are of course required.

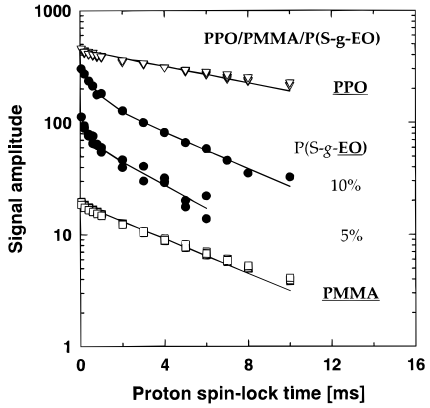

Figure 9. Proton $T_{1\rho}$(H) relaxation behavior at ~28 °C for PPO/PMMA/P(S-*g*-EO) 30/70/Φ, where Φ is 0, 5, and 10 (PEO resonance of P(S-*g*-EO)). The solid lines are single or biexponential fits to the data. For clarity, each decay is begun at a separate origin on the *y*-axis.

Ternary PPO/PMMA/P(S-*g*-EO) Blends. Results from the relaxation time measurements of the PPO/PMMA/P(S-*g*-EO) 30/70/5 and 30/70/10 blends are presented in Figure 9 ($T_{1\rho}$(H)), Table 2 ($T_{1\rho}$(H)), and Table 3 ($T_{1\rho}$(C)). As for the binary blends, the PEO $T_{1\rho}$(H) relaxation decay can be decomposed into two components with time constants ~0.5 and ~5 ms, respectively. The relaxation time for the slower component so obtained is close to $T_{1\rho}$(H) for PMMA (6 ms) which, in turn, is much shorter than that for PPO (14 ms). Carbon $T_{1\rho}$(C) is well described by an exponential decay with a single time constant of ~3 ms. We did not observe, again, any sign of side chain crystallinity, in agreement with the DSC and DMS results.

Overall, we thus find a striking similarity for the PEO relaxations for the blends in which PMMA are present (PMMA/PEO,[37,39] PMMA/P(S-*g*-EO), and PPO/PMMA/P(S-*g*-EO) of comparable compositions) (Figures 8 and 9 and Tables 2 and 3). Although the morphology differs in these blends, the relaxation behavior indicates that parts of the PMMA segments are spatially close to PEO segments so that the relaxation of the latter is changed as compared with that in PEO,[37,39] P(S-*g*-EO), and the PPO/P(S-*g*-EO) 100/10 blend.

It is then interesting to compare the molecular information from NMR with the previously discussed experimental finding of a micromechanical transition in the viscoelastic response, attributed to the interphase surrounding the PPO particles in the PMMA matrix. Although a theoretical simulation of the viscoelastic properties of the ternary blends using raw data for the pure blend constituents can qualitatively reproduce the micromechanical transition when an interphase is introduced, a decreased mobility of the interphase is required for a quantitative match of experimental data, as discussed before. Consequently, partial mixing between PEO side chains and PMMA molecules, as indicated by NMR, fits nicely with the dynamic mechanical results. In fact, the estimated hypothetical thickness of the interphase of ~50 nm (see section 3.1) is an order of magnitude larger than the effective spin diffusion distance probed in the proton $T_{1\rho}$(H) experiment. This means that if the interphase contained only pure copolymer, we would expect a relaxation behavior of the side chains similar to that of pure (amorphous) P(S-*g*-EO), in contrast to the experimental results. Molecular mixing within the interphase between PPO segments and the PS backbone of the copolymer is, of course, also possible. Due to the limited spectral

resolution, however, this latter interaction could not be investigated in the present work by NMR.

Finally, we note that the NMR results obtained so far are qualitative and cannot be used to distinguish between possible amorphous structures, such as copolymer-rich interphases or copolymer-rich domains within a certain phase. The NMR relaxation times were obtained for blends with relatively high copolymer concentrations of 5−10%. Both the SEM images (Figure 4) and the viscoelastic response (Figure 5) of the ternary blends indicate saturation of the interphase for copolymer concentrations in this range, and it is therefore probable that not all of the copolymer molecules are located at the interphase. A likely candidate for the excess copolymer is micelle formation within the PMMA matrix.

4. Conclusions

The results presented in this work show that a P(S-*g*-EO) graft copolymer, introduced at low amounts into immiscible PPO/PMMA (30/70) blends, is mainly concentrated at the interface. The average domain size of the dispersed PPO phase decreases continuously from ∼10 to ∼1 μm for increasing volume fractions of copolymer up to 10%, based on the total volume of PPO and PMMA. Thus, P(S-*g*-EO) acts in the same way as reducing the interfacial tension between the constituents.

When P(S-*g*-EO) is mixed with either of PMMA or PPO, only one glass transition is observed at a temperature lower than the glass transition temperature of the corresponding homopolymer. This is explained by at least a partial miscibility of the PS and the PEO part of the graft copolymer with the PPO and PMMA homopolymer, respectively. An interesting feature appears in the viscoelastic response upon the addition of copolymer to PPO/PMMA 30/70 blends. The ternary blends show an additional transition with a loss maximum at temperatures between 60 and 100 °C. The transition temperature depends on the amount of P(S-*g*-EO) added (a lower transition temperature for higher amounts of P(S-*g*-EO)). This micromechanical transition is attributed to the existence of an interphase with a distinct volume fraction and with its own characteristic properties.

The local features of the blends, with focus on the copolymer, were directly probed by solid-state CPMAS NMR. A detailed investigation of the carbon-13 PEO resonance reveals two dominating and slightly separated components in the pure P(S-*g*-EO). The observed difference in chemical shift (∼2 ppm) is attributed to the conformational difference for side chains in crystalline and amorphous regions, respectively. It was found that only amorphous PEO exists in the binary and ternary blends studied, in agreement with the dynamic mechanical data.

Proton and carbon NMR relaxations for the blends indicate that the average length scale of separation between PEO and PMMA is sufficiently small (∼nanometers) to cause a change in the PEO relaxation. Thus, the interphase between PPO and PMMA does not appear to be made up of pure P(S-*g*-EO) only, but rather some mixing with PMMA chains (and possibly also with PPO) is probably involved. However, we cannot rule out the possibility that parts of the NMR relaxations arise from copolymers in micelle formations, i.e., separated from the interphase.

Finally, the comparison of results from different experimental techniques for different length scales makes a valuable contribution to the understanding of the properties of the interphase.

Acknowledgment. We gratefully acknowledge the National Swedish Board for Industrial and Technical Development (NUTEK) for financial support of this work by the Consortium "Interface Interactions of Polymer Systems". The authors are also grateful to Marie Björklund for performing the SEC measurements and to Anders Mårtensson for performing the SEM experiments.

References and Notes

(1) Brown, H. R.; Char, K.; Deline, V. R.; Green, P. F. *Macromolecules* **1993**, *26*, 4155.
(2) Brown, H. R.; Char, K.; Deline, V. R. *Macromolecules* **1993**, *26*, 4164.
(3) Chen, C. C.; White, J. L. *Polym. Eng. Sci.* **1993**, *33*, 923.
(4) Gleinser, W.; Friedrich, C.; Cantow, H.-J. *Polymer* **1994**, *35*, 128.
(5) Tang, T.; Huang, B. *Polymer* **1994**, *35*, 281.
(6) Teyssié, Ph.; Fayt, R.; Jérôme, R. *Makromol. Chem., Macromol. Symp.* **1988**, *16*, 41.
(7) Thomas, S.; Prud'homme, R. E. *Polymer* **1992**, *33*, 4260.
(8) Bucknall, D. G.; Higgins, J. S. *Polymer* **1992**, *33*, 4419.
(9) Heuschen, J.; Vion, J. M.; Jérôme, R.; Teyssié, Ph. *Polymer* **1990**, *31*, 1473.
(10) Creton, C.; Brown, H. R.; Deline, V. R. *Macromolecules* **1994**, *27*, 1774.
(11) Ouhadi, T.; Fayt, R.; Jérôme, R.; Teyssié, P. *J. Polym. Sci., Polym. Phys. Ed.* **1986**, *24*, 973.
(12) Auschra, C.; Stadler, R. *Macromolecules* **1993**, *26*, 6364.
(13) Kim, H. C.; Nam, K. H.; Jo, W. H. *Polymer* **1993**, *34*, 4043.
(14) Fayt, R.; Jérôme, R.; Teyssié, P. *J. Polym. Sci., Polym. Lett. Ed.* **1981**, *19*, 79.
(15) Riess, G.; Jolivet, Y. *Copolymers, Polyblends and Composites*; Platzer, N. A. J., Ed.; American Chemical Society: Washington, DC, 1979; pp 243−256.
(16) Tucker, P. S.; Barlow, J. W.; Paul, D. R. *Macromolecules* **1988**, *21*, 2794.
(17) Shulz, A. R.; Beach, B. M. *Macromolecules* **1974**, *7*, 902.
(18) Li, X.; Hsu, S. L. *J. Polym. Sci., Polym. Phys. Ed.* **1984**, *22*, 1331.
(19) Rao, G. R.; Castiglioni, C.; Gussoni, M.; Zerbi, G.; Martuscelli, E. *Polymer* **1985**, *26*, 811.
(20) Bartczak, Z.; Martuscelli, E. *Makromol. Chem.* **1987**, *188*, 445.
(21) Maurer, F. H. J. *Polymer Composites*; Sedlacec, B., Ed.; W. de Gruyter & Co.: Berlin, 1986; p 399.
(22) Maurer, F. H. J. *Controlled Interphases in Composite Materials*; Ishida, H., Ed.; Elsevier: New York, 1990; pp 491−504.
(23) Eklind, H.; Maurer, F. H. J. *Polymer*, in press.
(24) Eklind, H.; Maurer, F. H. J. Submitted to *J. Polym. Sci., Polym. Phys. Ed.*
(25) Jannasch, P.; Wesslén, B. *J. Polym. Sci., Polym. Chem. Ed.* **1993**, *31*, 1519.
(26) Hirata, T.; Kashiwagi, T.; Brown, J. E. *Macromolecules* **1985**, *18*, 1410.
(27) Stejskal, E. O.; Schaefer, J.; Sefcik, M. D.; McKay, R. A. *Macromolecules* **1981**, *14*, 275.
(28) Schaefer, J.; Stejskal, E. O.; Buchdal, R. *Macromolecules* **1977**, *10*, 384.
(29) Zawada, J. A.; Ylitalo, C. M.; Fuller, G. G.; Colby, R. H.; Long, T. E. *Macromolecules* **1992**, *25*, 2896.
(30) Cholli, A. L.; Schilling, F. C.; Tonelli, A. E. *Solid State NMR of Polymers*; Mathias, L. J., Ed.; Plenum Press: New York and London, 1991; Chapter 6, p 117.
(31) VanderHart, D. L.; Earl, W. L.; Garroway, A. N. *J. Magn. Reson.* **1981**, *44*, 361.
(32) Dechter, J. J. *J. Polym. Sci., Polym. Lett. Ed.* **1985**, *23*, 261.
(33) Johansson, A.; Tegenfeldt, J. *Macromolecules* **1992**, *25*, 4712.
(34) Abragam, A. *The Principles of Nuclear Magnetism*; Oxford University Press: Oxford, 1961.
(35) McBrierty, V. J.; Douglass, D. C. *J. Polym. Sci., Macromol. Rev.* **1981**, *16*, 295.
(36) Schantz, S.; Maunu, S. L. *Macromolecules* **1994**, *27*, 6915.
(37) Schantz, S. *Polym. Mater. Sci. Eng.* **1994**, *71*, 209.
(38) Packer, K. J.; Pope, J. M.; Yeung, R. R.; Cudby, M. E. A. *J. Polym. Sci., Polym. Phys. Ed.* **1984**, *22*, 589.
(39) Schantz, S. Unpublished work.

MA950285D